ACI STRUCTURAL JOURNAL TECHNICAL PAPER

Title No. 119-S07

Three-Dimensional Macro-Modeling of Concrete Slabs Subjected to Missile Impact Loading

by Andac Lulec, Vahid Sadeghian, and Frank J. Vecchio

This study presents a macro-modeling method for analysis of reinforced and prestressed concrete slabs under soft and hard missile impact loads. The analysis method is based on the Modified Compression Field Theory, incorporating a rational approach based on fundamental principles of solid mechanics and eliminating the need for extensive material characterizations. An iterative self-calibrating procedure was developed and implemented into a finite element analysis framework to systematically determine element erosion limits and damping coefficients, expanding the applicability range of the analysis method. Two different implementation methods for incorporating damping into the analysis formulation are investigated. Special considerations are given to modeling strain rate effects and advanced material mechanisms. The performance of the analysis method is evaluated through modeling 12 missile impact tests from the literature as well as conducting a series of analytical parametric studies. The analysis results show that the proposed modeling method is an efficient and reliable approach for analysis of concrete slabs under impact loading capable of capturing localized damages and shear failures.

Keywords: element erosion; finite element modeling; impact loading; nonlinear analysis; reinforced concrete slabs.

INTRODUCTION

The development of analysis tools for the safety and performance assessment of concrete structures under impact loading has drawn the interest of many researchers and engineers due to the increased number of natural and accidental hazards worldwide, and the need to develop performance-based design guidelines for impact-resistant structures. In current practice, empirical formulae and complex hydrocodes are the most widely used methods for the impact analysis of concrete structures. Empirical formulae are typically based on a simplification of the structure to a single-degree-of-freedom (SDOF) system and are commonly used by engineers for design purposes. While penetration depth, the occurrence of perforation, and time-displacement response can be obtained with these formulae, they are incapable of providing detailed results such as the damage condition or failure mode. Moreover, they are inapplicable to structures with complex geometries. A detailed review of the empirical formulae available in the literature is provided by Lulec et al.[1]

On the other hand, highly sophisticated finite element (FE) procedures such as hydrocodes[2,3] can overcome the problems associated with simplification of the behavior, but they require modeling of both the target and missile in great detail. The tremendously increased number of elements and degrees of freedom (DOFs) used in the analyses result in much longer modeling and computation times. Moreover, a large number of reinforced or prestressed concrete material properties usually have to be entered as input parameters, or calibrated, many of which are not typically known. As a result, the advantage of the hydrocodes in terms of accuracy and detail of results decreases due to modeling complexity, longer computational time periods, and uncertainty in material characterization; in some cases, these complications render hydrocodes impractical for practical analysis and design purposes.

In 2010, the VTT Technical Research Center of Finland and the Institut de Radioprotection et de Sûreté Nucléaire organized a blind prediction competition to evaluate the accuracy of existing analysis tools in computing the response of two reinforced concrete (RC) slab specimens, one subjected to soft missile impact and the other one tested under hard missile impact.[4,5] In soft missile impacts, the missile deforms significantly, whereas in hard missile impacts, the missile shows small or negligible deformation causing significant local deformation on the target in addition to the overall dynamic response of the target. Twenty-seven participating teams submitted predictions using a variety of analysis approaches. Significant variations were observed among the predictions for both tests, especially for the hard missile impact test. For example, predictions for the missile residual velocity, which is one of the key parameters for punching/perforation tests, had a coefficient of variation (COV) of 274%. The high level of variation can be attributed to two factors: 1) difficulties involved in defining suitable element erosion criteria and limits; and 2) the inability of the analysis tools in capturing shear mechanisms which are often dominant in the overall behavior of concrete structures under hard missile impact loading. Two years later, at the IRIS2012 workshop, the participating teams resubmitted their predictions for the same test specimens with the advantage of knowing the results.[5] A significant improvement in predictions was observed; however, the COV of predictions remained high (for example, the COV of the missile residual velocity was 53%). Regarding the analysis approaches taken, 82% and 64% of the teams used complex hydrocodes in IRIS2010 and IRIS2012, respectively. Most of these teams modeled the target in great detail using 500,000 to 1,000,000 DOFs, which required significant modeling and computational efforts.

The persistent, significant variations among the predictions in both workshops show that there remains a need for

ACI Structural Journal, V. 119, No. 1, January 2022.

MS No. S-2020-355.R1, doi: 10.14359/51734189, received May 17, 2021, and reviewed under Institute publication policies.

accurate and practically repeatable analytical tools, particularly in the middle ground between the SDOF methods and highly sophisticated hydrocodes. As an alternative analytical tool, this study proposes a macro-modeling approach for reinforced and prestressed concrete slabs which is capable of accurately computing both the flexural and shear behavior under impact loads using reasonable mesh sizes without requiring the calibration of material models and analysis parameters.

RESEARCH SIGNIFICANCE

Generally, available methods for impact analysis of concrete structures either oversimplify the behavior of structures or require significant modeling efforts. Additionally, determining damping ratios and element erosion limits, which are important parameters in the analysis of structures under impact, is a challenging task. These values can vary significantly from one study to another. This paper presents an alternative analysis approach that is capable of computing the structural response, including local damages due to shear forces, in a practical manner with good accuracy. A systematic approach is developed for determining damping ratios and element erosion limits which facilitates analysis of structures and expands the applicability range of the analysis method.

ANALYSIS METHODOLOGY

Overview

To solve the equation of motion and carry out nonlinear dynamic analyses, a modified version of Newmark's time integration method developed by Saatci and Vecchio[6] was implemented in VecTor3,[7] a three-dimensional (3D) nonlinear FE analysis software for RC structures. The modified Newmark's method represents the solution of the equation of motion with the same format as the Hookes' law equation used for static analyses (that is, force equals stiffness times displacement)

$$\left(\left[k_{i+1}^{static}\right]+\left[k_{i+1}^{dyn}\right]\right)\left\{u_{i+1}\right\}=\left\{p_{i+1}^{static}\right\}+\left\{p_{i+1}^{dyn}\right\} \tag{1}$$

where

$$\left[k_{i+1}^{dyn}\right]=\frac{[m]+[c_{i+1}]\gamma\Delta t}{\beta\Delta t^2} \tag{2}$$

$$\left\{p_{i+1}^{dyn}\right\}=\left\{p_{i+1}\right\}+\frac{[m]+[c_{i+1}]\gamma\Delta t}{\beta}\left(\frac{\{u_i\}}{\Delta t^2}+\frac{\{\dot{u}_i\}}{\Delta t}+\frac{\{\ddot{u}_i\}}{2}\right)-[c_{i+1}](\{\dot{u}_i\}+vt\{\ddot{u}_i\})-[m]\{\ddot{u}_i\} \tag{3}$$

where $[k^{static}]$ and $[k^{dyn}]$ are the static secant stiffness matrix and the equivalent dynamic stiffness matrix; $\{u\}$, $\{\dot{u}\}$, and $\{\ddot{u}\}$ are the displacement, velocity and acceleration vectors; $\{p^{static}\}$ and $\{p^{dyn}\}$ are the static total load vector and the equivalent dynamic load vector; $[m]$ and $[c]$ are the mass and damping matrixes; γ and β are coefficients for the variation of acceleration over the time step; Δt is the time step size; and subscripts i and $i + 1$ indicate the time step of variables. The mass matrix is defined as a diagonal matrix where the total mass of a structure is evenly distributed and assigned to the nodes of the FE model. The damping matrix is defined as a linear combination of the mass and stiffness matrixes according to Rayleigh damping.[8]

The secant stiffness matrix at the element level, $[k]$, is related to the secant stiffness matrix at the material-level, $[D]$, using the following equation

$$[k]=\int_{Vol}[B]^T[D][B]dV \tag{4}$$

where $[B]$ is the strain function matrix, which depends on the element type used for the FE analysis. The secant stiffness matrix for the reinforced concrete material, $[D]$, is defined according to the Disturbed Stress Field Model (DSFM),[9] which is an improved version of the Modified Compression Field Theory (MCFT)[10]

$$[D]=[T_c]^T[D_c'][T_c]+\sum_{i=1}^{n}[T_s]_i^T[D_s']_i[T_s]_i \tag{5}$$

where $[D_c']$ is the concrete secant stiffness matrix in the principal stress directions; $[D_s']_i$ is the secant stiffness matrix for the i-th component of reinforcement along its longitudinal direction; and $[T_c]$ and $[T_s]_i$ are the coordinate transformation matrixes to transform the concrete and reinforcement stiffness values into the reference coordinate system. In the MCFT model, the secant stiffness matrixes for the concrete and the reinforcement are defined as the following

$$[D_c']=\begin{bmatrix}\bar{E}_{c1}&0&0&0&0&0\\0&\bar{E}_{c2}&0&0&0&0\\0&0&\bar{E}_{c3}&0&0&0\\0&0&0&\bar{G}_{c12}&0&0\\0&0&0&0&\bar{G}_{c13}&0\\0&0&0&0&0&\bar{G}_{c23}\end{bmatrix};[D_s']_i=\begin{bmatrix}\rho_i\bar{E}_{si}&0&0&0&0&0\\0&0&0&0&0&0\\0&0&0&0&0&0\\0&0&0&0&0&0\\0&0&0&0&0&0\\0&0&0&0&0&0\end{bmatrix} \tag{6}$$

where $\bar{E}_{cm}$ is the concrete secant modulus in the m-th principal stress direction; $\bar{G}_{cmn}$ is the concrete secant shear modulus on the mn principal plane; and ρ_i and $\bar{E}_{si}$ are the reinforcement ratio and secant modulus of the i-th reinforcement component. The secant moduli for the concrete and the reinforcement are equal to

$$\bar{E}_{cm}=\frac{f_{cm}}{\varepsilon_{cm}};\bar{G}_{cmn}=\frac{\bar{E}_{cm}\bar{E}_{cn}}{\bar{E}_{cm}+\bar{E}_{cn}};\bar{E}_{si}=\frac{f_{si}}{\varepsilon_{si}} \tag{7}$$

where f_{cm} and ε_{cm} are the stress and net strain in the m-th principal direction in the concrete and f_{si} and ε_{si} are the stress and net strain in the i-th component of reinforcement. The net strains in the concrete and reinforcement (ε_c, ε_s) are calculated by subtracting the elastic and plastic strain offsets from the total strains as shown in Eq. (8)

$$\varepsilon_c=\varepsilon_c^t-\left(\varepsilon_c^e+\varepsilon_c^p+\varepsilon_c^s\right);\varepsilon_s=\varepsilon_s^t-\left(\varepsilon_s^e+\varepsilon_s^p\right) \tag{8}$$

where subscripts c and s indicate concrete and steel; ε^t is the total strain; ε^e is the elastic strain offset (for example, shrinkage in concrete or prestressing in steel); ε^p is the plastic strain offset (for example, permanent strains due to

unloading); and ε_c^s is the strain due to slip along the crack. Using material constitutive models, stresses in the concrete and the reinforcement can be determined from the net strains. The stresses will then be used to compute the stiffness matrix at the material-level, as discussed earlier. Strains due to slip along the crack and material constitutive models used in this study will be discussed further in the next section. For more information about the analysis formulation refer to Lulec.[11]

This study aims to further develop the dynamic analysis method presented earlier and assess its performance for analysis of concrete structures subjected to soft and hard missile impact loading. This requires the addition of two new features to the existing analysis formulation: 1) an element erosion capability that can be systematically applied to various structures to capture local damage, especially under hard missile impacts; and 2) an algorithm for updating the damping matrix that ensures stability of the numerical solution without introducing excessive damping mechanisms into the structural system. Additionally, this study investigates the accuracy of the analysis method in capturing shear behavior which typically plays a critical role in the performance of concrete structures under impact loading. The key parts of the analysis method are discussed in the following.

Material constitutive models

Several material constitutive models are adapted from the literature to account for important mechanisms influencing the response of concrete and reinforcement under impact conditions. The uniaxial compressive response of concrete is considered according to the Hoshikuma et al.[12] model, which uses a nonlinear response prior to the peak strength and assumes a bilinear response for the post-peak behavior, as shown in Fig. 1 and expressed in the following equations

$$f_{cm} = \begin{cases} E_c \varepsilon_{cm} \left[1 - \frac{1}{k} \left(\frac{\varepsilon_{cm}}{\varepsilon_p} \right)^{k-1} \right] & |\varepsilon_{cm}| \le |\varepsilon_p| \\ -\left[f_p + \frac{11.2}{\rho_s f_{yh} / f_c'^2} (\varepsilon_{cm} - \varepsilon_p) \right] \le -0.2 f_p & |\varepsilon_{cm}| > |\varepsilon_p| \end{cases} \tag{9}$$

$$k = \frac{E_c}{E_c - \bar{E}_p}; \bar{E}_p = \frac{f_p}{\varepsilon_p} \tag{10}$$

where f_{cm} and ε_{cm} are the compressive stresses and strains in the m-th principal direction; E_c is the Young's modulus of concrete; f_p is the peak compressive strength; ε_p is the strain at the peak compressive stress; and ρ_s and f_{yh} are the ratio and yield strength of shear reinforcement, respectively. f_p and ε_p are determined by adjusting the uniaxial concrete cylinder strength (f_c') and the corresponding strain (ε_o) to account for the confinement and compression softening effects. The compression softening effect is considered using a model developed by Vecchio and Collins[13] as provided in the following

$$f_p = \beta f_c'; \varepsilon_p = \beta \varepsilon_o \tag{11}$$

$$\beta = \frac{1}{1 + 0.55 C_d}; C_d = \begin{cases} 0 & \frac{-\varepsilon_{cn}}{\varepsilon_{cm}} \le 0.28 \\ 0.35 \left(\frac{-\varepsilon_{cn}}{\varepsilon_{cm}} - 0.28 \right)^{0.80} & \frac{-\varepsilon_{cn}}{\varepsilon_{cm}} > 0.28 \end{cases} \tag{12}$$

where ε_{cn} is the concrete tensile strain in the n-th principal direction. The tensile response of concrete is assumed linear elastic prior to cracking. After cracking, the tension stiffening model proposed by Bentz[14] is used to account for tensile stresses in the concrete between the cracks in the vicinity of the reinforcement

$$f_{cn} = \frac{f_{cr}}{1 + \sqrt{c_t \varepsilon_{cn}}} \tag{13}$$

where f_{cn} is the concrete tensile stress in the n-th principal direction; f_{cr} is the concrete cracking strength; and c_t is a factor that depends on the ratio, diameter, and inclination of the reinforcement. The MCFT model limits the concrete tensile stress by the ability of the reinforcement to carry the stress across the crack

$$f_{cn} \le \sum_{i=1}^{n} \rho_i \left(f_{yi} - f_{si} \right) \cos^2 \theta_i \tag{14}$$

where ρ is the reinforcement ratio; f_y and f_s are the average and yield stress in the reinforcement, respectively; θ is the angle between the normal to the crack and the reinforcement; and subscript i indicates that the parameters are for

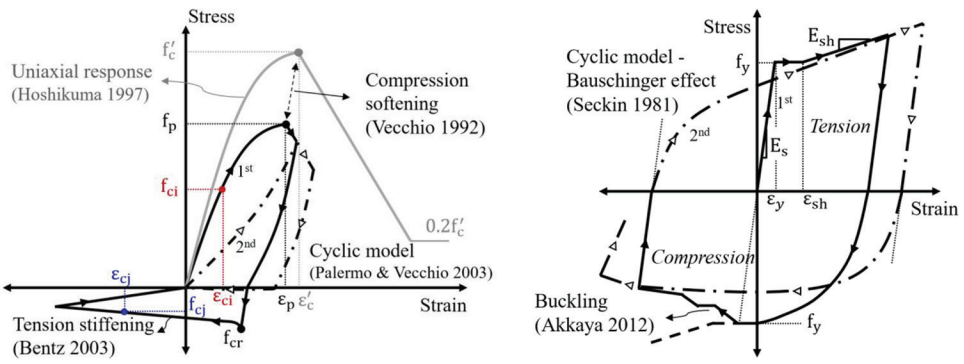

Fig. 1—Material models used for concrete (left) and reinforcement (right).

the *i*-th reinforcement component. While tensile stresses are zero at the crack, local shear stresses exist along the crack surface to satisfy force equilibrium. The local shear stresses (v_c) are calculated according to the MCFT model as follows

$$v_c = \sum_{i=1}^{n} \rho_i \left(f_{scri} - f_{si} \right) \cos\theta_i \sin\theta_i \tag{15}$$

where f_{scr} is the local reinforcement stress at the crack determined using equilibrium relationships as provided in the MCFT model. Shear deformations resulted from the local shear stresses at the crack are calculated based on a model proposed by Walraven[15] and are incorporated into the analysis formulation as slip strains according to Eq. (8). The cyclic response of concrete is considered using the Palermo and Vecchio[16] model, which follows a nonlinear unloading response for both tension and compression and is capable of computing plastic offset strains due to internal damage.

The cyclic response of reinforcement is calculated using the Seckin[17] model, which captures the premature yielding of the reinforcement upon load reversal after the initial yielding (that is, the Bauschinger effect). This model assumes a trilinear backbone stress-strain relationship, a linear unloading response, and a nonlinear reloading response with the Bauschinger effect. The backbone stress-strain relationship is presented as follows

$$f_s = \begin{cases} E_s \varepsilon_s & \varepsilon_s \le \varepsilon_y \\ f_y & \varepsilon_y < \varepsilon_s \le \varepsilon_{sh} \\ f_y + E_{sh}\left(\varepsilon_s - \varepsilon_{sh}\right) & \varepsilon_s > \varepsilon_{sh} \end{cases} \tag{16}$$

where f_s and ε_s are the stress and strain in the reinforcement, respectively; f_y and E_s are the yielding strength and initial elastic modulus of the reinforcement, respectively; ε_{sh} is the strain at which the strain hardening region begins; and E_{sh} is the tangent modulus of the strain-hardening region. Additionally, the Akkaya et al.[18] model is employed to account for inelastic buckling of the reinforcement in compression. The material models used for the concrete and reinforcement are summarized in Fig. 1.

In all the verification studies presented in this paper, the same set of material models were used to eliminate problems associated with material characterization and to assess the applicability of the analysis method to different types of impact tests.

Strain rate effect

In hydrocodes, the strain rate effect is usually incorporated into the material constitutive models. With simplified analysis tools, however, the strain rate effect is mostly considered using dynamic increase factors (DIFs) applied to the material properties. When using SDOF models, the DIFs should be applied to both the concrete and reinforcement because of the limitations of these models in considering the geometry of the structure and inertial effects. For FE analyses, however, the DIFs for concrete may not be needed because the inertial effects and triaxial confinement stress conditions that are typically induced under dynamic loads will naturally result in elevated strengths. Thus, using DIFs for reinforcement alone is usually more suitable; this approach is employed in the FE analysis method proposed herein. Through a parametric study which will be presented in the "Verification Studies" section, it is shown that considering the strain rate effect for both concrete and steel results in an overly stiff response. The concrete and steel strain rate effects are calculated according to the 2010 *fib* Model Code[19] and the Malvar-Crawford[20] model, respectively. The 2010 *fib* Model Code provides DIF formulations for the concrete compressive and tensile strength, the modulus of elasticity, and the strain at the peak strength. The Malvar-Crawford model provides equations to calculate the increase in the yield and ultimate strength of the reinforcement as a function of the strain rate.

Damping and element erosion

In addition to the strain rate effect, damping and element erosion are the other important factors in the dynamic analysis of structures under impact loads. Damping is usually used to include additional energy dissipating mechanisms and to reduce the instability of the numerical solution. Element erosion criteria are defined to simulate physical loss of material due to local damage under hard missile impacts. Although significant efforts have been made to investigate the influence of various damping values and element erosion limits on the structural response, there has not been a systematic method proposed for determining these two parameters applicable to different types of impact tests. Luccioni and Aráoz[21] reviewed element erosion algorithms used in blast and impact analyses in the literature and found that not only is there no consensus among researchers on what erosion criterion should be used, but also that erosion limits used in various studies vary significantly.

In this study, a self-calibration procedure is proposed for determining the damping coefficients and element erosion limits in a consistent manner. With this method, the damping coefficients and erosion limits are iteratively modified according to the time-missile velocity response and the deformed geometry of the target. Initially, damping coefficients with small values are chosen to avoid introducing excessive energy dissipation to the system, and element erosion limits with high values are selected to avoid premature element erosion and to allow the computation of softening in the structural response through constitutive material models. The initial values are selected according to the recommendations of Luccioni and Aráoz.[21] Generally, these initial values yield highly deformed elements and noisy time-missile velocity relations with abrupt increases in missile velocity. The velocity increases indicate an energy gain within the system, which is physically impossible. To reduce these abrupt velocity increases and abnormal deformation of elements, the damping matrix coefficients are gradually increased and the element erosion limits gradually reduced. The calibration is deemed complete when the time-missile velocity relation first become smooth and no abnormally deformed elements remain. The self-calibration procedure can be either conducted manually or implemented into the analysis formulation, as shown in Fig. 2.

Although the proposed analysis method does not explicitly consider the viscous response of concrete at the material

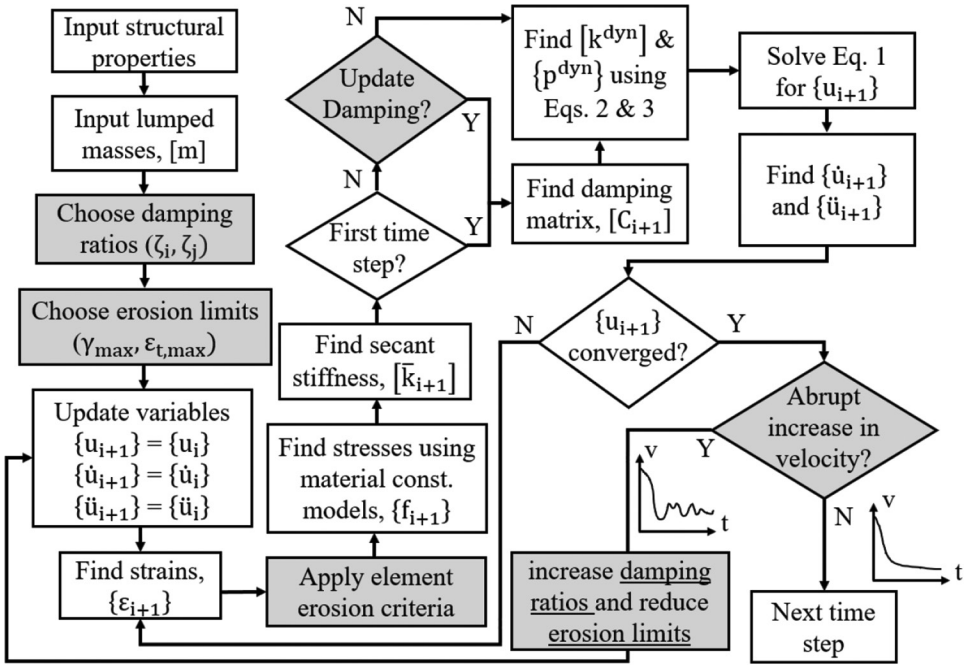

Fig. 2—Overview of analysis algorithm (new steps are highlighted in gray).

level, it captures the majority of energy dissipation mechanisms through permanent deformations defined in material hysteretic responses and mechanisms involved in opening and closing of concrete cracks. To ensure the stability of the numerical solution, a small amount of damping is added to the system according to Rayleigh damping, in which the damping matrix (C) is proportional to the mass (m) and stiffness (k) matrixes, as expressed in Eq. (17)

$$[C] = a_0[m] + a_1[k] \tag{17}$$

where a_0 and a_1 are coefficients for the mass and stiffness matrixes, respectively, obtained from

$$a_1 = \frac{2\zeta_j\omega_j - 2\zeta_i\omega_i}{\omega_j^2 - \omega_i^2}; a_0 = 2\zeta_i\omega_i - a_1\omega_i^2 \tag{18}$$

where ζ and ω are modal damping ratio and angular frequency, respectively; and subscripts i and j indicate two arbitrary modes.

A similar approach was successfully used by other researchers to account for energy dissipation mechanisms in RC structures without explicit consideration of the viscous response of materials. For example, Saatci and Vecchio[6] analyzed a series of RC beam specimens under impact loads and demonstrated that because of mechanisms such as concrete cracking and material hysteresis, considerable damping takes place in the dynamic response even if no additional viscous damping is introduced into the model.

Two different methods are considered for implementation of the damping matrix into the analysis formulation. In the first method, both the damping coefficients (a_0 and a_1) and damping matrix are determined from the initial stiffness matrix; while in the second method, the damping coefficients are computed by using the initial stiffness, but the damping matrix is calculated using the updated secant stiffness matrix, which accounts for nonlinearity in the response. Hereafter, the first method will be referred to as the "constant damping method" and the second method will be called the "updating damping method."

To capture local damage caused by shear failure, element erosion criteria based on the shear strain (γ_{max}) and the principal tensile strain ($\varepsilon_{t,max}$) are used for hard missile impact analyses, as suggested by Luccioni and Aráoz.[21] Erosion criteria limits are determined according to the self-calibration procedure presented earlier. Consequently, any concrete element within the model having an absolute value of shear strain or principal tensile strain larger than the erosion criteria limits is removed from the calculations by assigning a small stiffness value. However, the lumped masses assigned to the nodes are kept constant, retaining the conservation of mass and momentum. Additionally, rupture of the reinforcement is modeled with an element erosion criterion based on the ultimate strain value of the truss element. Any truss element having a larger strain than the ultimate strain value reported in the experiments is eroded. Figure 2 shows an overview of the analysis algorithm with the new computational steps for the damping matrix and element erosion highlighted in gray.

VERIFICATION STUDIES

All analyses presented in this section were performed using the same material constitutive models, element erosion criteria, and analysis options, and no attempt was made to fine-tune the results.

Reinforced concrete tests

The two RC slab specimens that were the subject of the blind prediction competition,[4,5] discussed in the Introduction, were modeled in this section. The first specimen (VTT-B1) was tested under a soft missile impact with a missile mass and impact velocity of 50 kg (110.2 lb) and 110 m/s (360.9 ft/s), respectively. The second specimen

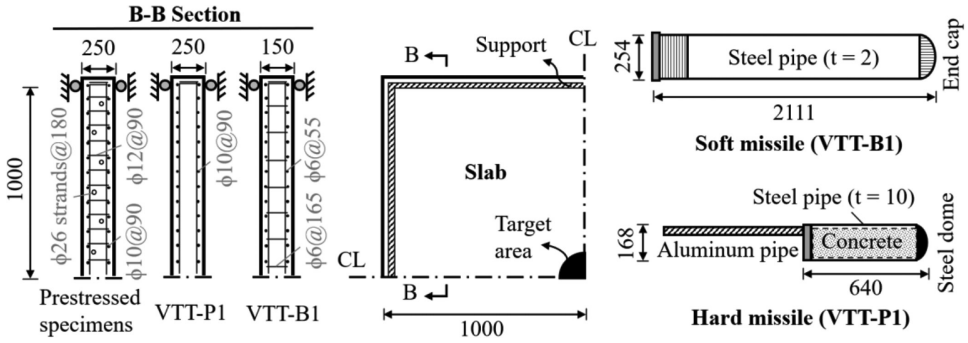

Fig. 3—Missile and target details of impact tests. (Note: Dimensions in mm; 1 mm = 0.0394 in.)

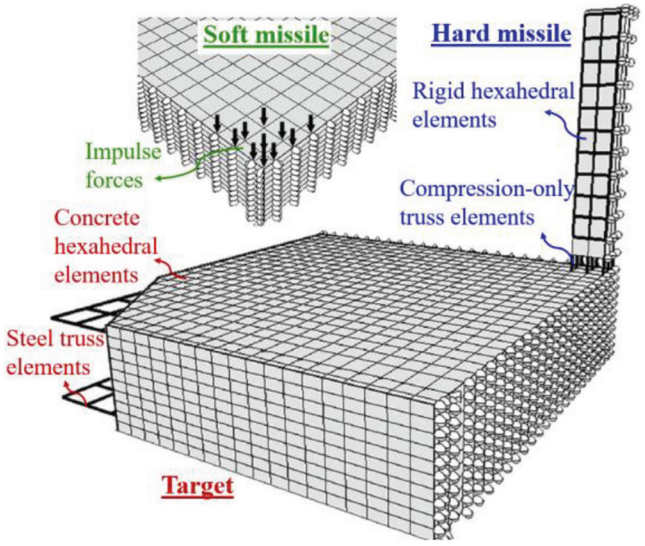

Fig. 4—FE models of RC slabs subjected to soft and hard missiles.

(VTT-P1) was subjected to a hard missile impact with a missile mass and impact velocity of 47 kg (103.6 lb) and 135.9 m/s (445.9 ft/s), respectively. Both slabs were simply supported along all four edges with a clear span of 2000 mm (78.74 in.) in both directions. The VTT-B1 specimen had top and bottom orthogonal in-plane reinforcement, each layer consisting of 38 ϕ6 reinforcing bars with a spacing of 55 mm (2.16 in.) in both directions. Also, ϕ6 single-leg stirrups, spaced at 165 mm (6.50 in.) in each direction, were used as the shear reinforcement. For the VTT-P1 specimen, each in-plane reinforcement layer consisted of 24 ϕ10 reinforcing bars with a spacing of 90 mm (3.54 in.) in both directions. This specimen had no shear reinforcement. The thickness of the VTT-B1 specimen was 150 mm (5.90 in.), and the thickness of the VTT-P1 specimen was 200 mm (7.87 in.). The clear concrete cover for both specimens was equal to 10% of their thickness. Figure 3 shows the geometry and reinforcement details of the two specimens and the geometry of the missiles.

Taking advantage of double symmetry, only one-quarter of each slab was modeled and restrained on the axes of symmetry using nodal restraints. The concrete components of the VTT-B1 slab were modeled with 4410 eight-noded hexahedral elements using a mesh of 55 x 55 x 15 mm (2.16 x 2.16 x 0.59 in.). The in-plane reinforcement was modeled by 1520 discrete truss elements, and the shear reinforcement was modeled as smeared reinforcement within the concrete elements. For the VTT-P1 slab, 5760 hexahedral elements and 1104 truss elements were used, resulting in a mesh size of 45 x 45 x 25 mm (1.77 x 1.77 x 0.98 in.).

The soft missile used for testing the VTT-B1 slab was not modeled because the analysis procedure is not capable of modeling the buckling behavior of a steel tube. Instead, the missile impact was modeled as an impulse load acting on the corner of the specimen, as shown in Fig. 4. The impulse force time-history was calculated according to the Riera method.[22] For the VTT-P1 slab, the concrete fill of the hard missile was modeled with 48 rigid hexahedral elements, and the steel tube of the missile was modeled with 94 truss bars. The missile was connected to the specimen with nine compression-only truss bars. In terms of loading, a quarter-mass of the missile was evenly distributed to nodes within the missile as lumped masses, and an initial velocity was assigned to these masses. Figure 4 shows the FE models used for the slabs subjected to the soft and hard missiles.

For the VTT-B1 slab, 0.25% and 0.5% were assigned as the modal damping ratios for the first and second modes (ζ_1 and ζ_2 in Eq. (18)), which were the lowest values producing a numerically stable solution based on the self-calibration procedure. A series of analyses were performed to investigate the influence of the reinforcement modeling method, strain rate effects, damping ratios, damping implementation method, and time step size on the structural performance. The displacement-time responses obtained from the analyses and the experiment for the center of the VTT-B1slab are presented in Fig. 5.

Reinforcement modeling method—To examine the effect of reinforcement modeling, the in-plane reinforcing bars were modeled as smeared reinforcement instead of discrete truss elements. The peak displacement value obtained from the model with the truss elements was 28.9 mm (1.14 in.), which was identical to the experimental value. As can be seen from Fig. 5(a), the response of the model with truss elements closely matched with the experimental behavior until the peak displacement. However, the period obtained from the simulation started to shift from the actual period of the specimen after the first peak. One possible cause of the discrepancy between the periods is that the stiffness and vibration of the restraint frame are not being taken into account because the support rig is not modeled.

The model with the smeared in-plane reinforcement overestimated the peak displacement with an error of 25%. The

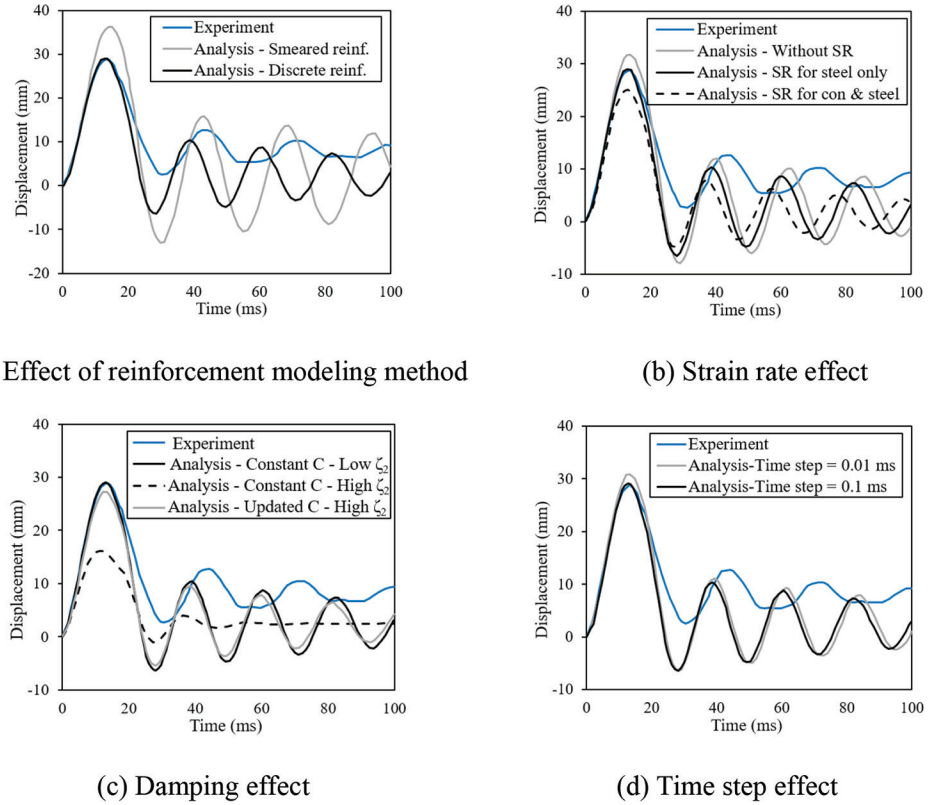

Fig. 5—Displacement-time responses for VTT-B1 slab. (Note: 1 mm = 0.0394 in.)

discrepancy between the results obtained from the models with different reinforcement modeling approaches was caused by the number of concrete elements lying in the tension-stiffening zone. The analysis assumes that concrete elements in the vicinity of 7.5 bar diameters of a truss element are within the tension-stiffening zone. On the other hand, for the model where the reinforcement is modeled as smeared reinforcement, the tension-stiffening zone is limited to the concrete elements having the smeared reinforcement. Consequently, the model with the truss bars has more concrete elements in which tension-stiffening effects are considered, yielding a stiffer response than the model with the smeared reinforcement. Although the model with smeared reinforcement yielded less-accurate results, it may be preferred due to practical reasons such as ease in modeling and conservative results.

Strain rate effects—The influence of strain rate effects was examined by three analyses: one without any strain rate effects; one with the strain rate effects for steel only; and one where the strain rate effects are considered for both concrete and steel. As can be observed from Fig. 5(b), the analysis without any strain rate effects overestimated the peak displacement with an error of 9.5%. On the other hand, the analysis considering strain rate effects for both the concrete and steel underestimated the peak displacement with an error of –13.5%. This supports the argument made in the "Analysis Methodology" section that considering the strain rate effects for both the concrete and steel in FE analyses can result in overly stiff structural responses.

Damping ratios and implementation method—Three different analyses were performed: a constant damping matrix with damping ratios of 0.25 and 0.5% for the first two modes; a constant damping matrix with damping ratios of 4 and 18%; and an updated damping matrix with damping ratios of 4 and 18%. It should be noted that the selected damping ratios are only for comparison purposes and do not represent actual values. As can be seen from Fig. 5(c), the damping ratios and the method used for calculation of the damping matrix had a significant influence on the accuracy of the displacement-time response. The analysis with the constant damping matrix and damping ratios of 0.25 and 0.5% produced a peak displacement of 28.9 mm (1.14 in.). Using a constant damping matrix with significantly higher damping ratios of 4% and 18% increased the damping matrix coefficients for mass and stiffness (a_0 and a_1) with a ratio of 1.6 and 38.3, respectively. Consequently, the peak displacement became 16.1 mm (0.63 in.), which is 56% of the value obtained from the previous analysis case. On the other hand, using an updated damping matrix with the same damping ratios yielded a peak displacement of 27.2 mm (1.07 in.), which is 94% of the one calculated in the initial analysis case. Therefore, the influence of significantly larger damping ratios diminishes when using an updated damping matrix. Note that the mass portion of the damping matrix is always constant; thus, a_0 should be kept small to avoid introducing excessive amounts of damping to the system.

Time step size—The influence of the time step used was investigated through two different analyses; one with a time step of 0.1 ms which was the base simulation case, and another one with a time step of 0.01 ms. As can be seen from Fig. 5(d), the displacement-time history responses obtained from the two analyses with different time step sizes are close to each other, which shows that the time step of 0.1 ms is adequately small for accurate analysis of the specimen.

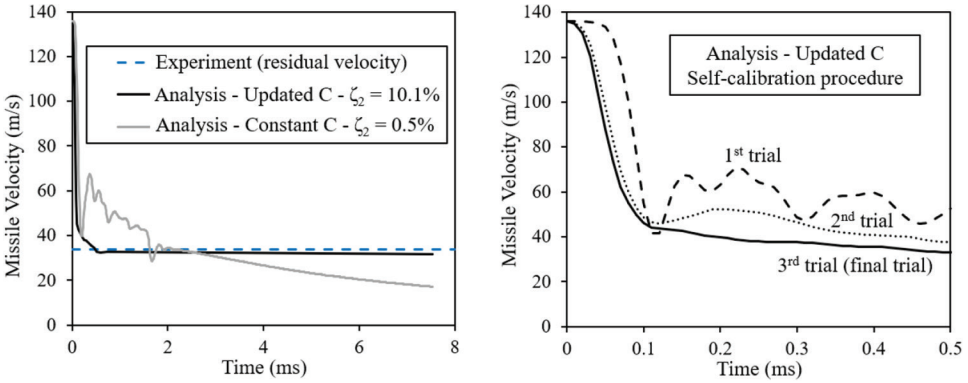

Fig. 6—Missile velocity-time responses for VTT-P1 slab: damping effect (left) and iterative self-calibration procedure (right). (Note: 1 m/s = 3.281 ft/s.)

For the VTT-P1 slab, when using the self-calibration method, a value of 0.16 was found to be suitable for the element erosion limit for both principal tensile and shear strains. The time step chosen was 0.01 ms, which was small enough to satisfy numerical stability. The final damping ratios obtained from the self-calibration method for the first and second modes were 2.6% and 10.1%, respectively. Although the damping ratio of the second mode was high, because of updating the damping matrix in each time step of the analysis, the damping effect diminished quickly, resulting in no excessive damping in the system. To demonstrate the advantage of using the updating damping method, a similar analysis was performed using the constant damping method where a much lower damping ratio was used for the second mode (ζ_1 = 2.6% and ζ_2 = 0.5%). As shown in Fig. 6, the missile residual velocity reached a constant value with the updating damping method (with high damping ratios); with the constant damping method (with low damping ratios), the missile velocity continued to decrease even after the missile perforated through the target which was not realistic. The residual velocity obtained from the analysis with the updating damping method was 31.8 m/s (104.3 ft/s), sufficiently close to the experimental value of 33.8 m/s (110.9 ft/s) with an error of –1.5% with respect to the initial velocity.

Figure 6 also shows the three analysis trials used for the self-calibration procedure to obtain suitable damping coefficients and element erosion limits. The first analysis trial used small damping coefficients (ζ_1 = 0.2% and ζ_2 = 0.3%) and a large element erosion limit (0.50) to avoid introducing excessive damping to the system and eliminating elements prematurely. For the second and third analysis trials, the damping coefficients gradually increased (ζ_1 = 1.9% and 2.6%; ζ_2 = 7.3 and 10.1%) and the element erosion limit gradually reduced (0.40 and 0.16) until no abrupt increase in missile velocity nor abnormal deformation in elements was observed.

The damage surfaces and deformed shapes obtained from the analysis and experiment are compared in Fig. 7. The analytical and experimental results matched sufficiently well with each other, especially for the back face. The analysis was able to capture the shear cone observed in the test specimen. The hole on the front face obtained from the analysis was slightly larger than that experimentally observed; this was due, in part, to the coarseness of the mesh size which influenced the size of the area depleted by element erosion.

In terms of the computational efficiency, the analysis of the VTT-P1 specimen using the proposed modeling method took 18.5 hours on a quad-core personal computer. The average analysis time of four teams that attended the IRIS2010 workshop and modeled the same specimen in LS-DYNA was approximately 121.5 hours. Assuming that the LS-DYNA analyses were also conducted on similar personal computers, it can be concluded that the proposed analysis method is substantially more computationally efficient than hydrocodes. A more detailed comparison between the two methods requires knowing the exact computing power used for the LS-DYNA analyses. In terms of the model size, most of the teams that used hydrocodes required between 500,000 and 1,000,000 DOFs to model each of the slab specimens. The proposed modeling methodology required only approximately 6500 elements to analyze the specimens. Lastly, hydrocodes often require extensive characterization of material properties, which are typically unknown. For example, a detailed definition of a typical concrete material model in LS-DYNA requires between 12 to 50 input parameters, many of which are difficult to estimate. In the proposed analysis method, however, only basic input parameters are needed to define the material models. For example, the concrete model used for the slab analyses was defined based on only three input parameters: the uniaxial compressive strength, the strain at peak compressive strength, and the Young's modulus.

Prestressed concrete tests

In addition to the IRIS2010 specimens, ten hard missile impact tests were carried out at the VTT testing facility to evaluate the influence of the transverse and prestressing steel.[23,24] The aim of the first six tests (Specimens A to F) was to examine the punching behavior and level of deformation of prestressed concrete slabs when the missile velocity was less than the perforation.[23] The remaining four tests (Specimens G to J) focused on assessing the perforation capacity of the target.[24] The geometry of the specimens and the base reinforcement details were the same as those of the VTT-P1 slab (refer to Fig. 3). Additionally, Specimens D, E, F, H, I, and J had 12 mm (0.47 in.) T-headed bars are located at the intersection of the in-plane reinforcement bars as shear

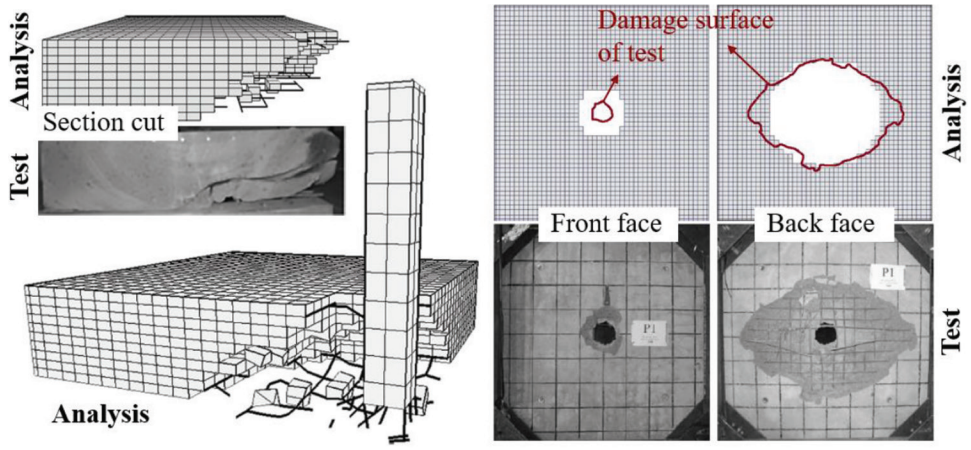

Fig. 7—Analytical and experimental damage surfaces and deformed shapes for VTT-P1 slab.

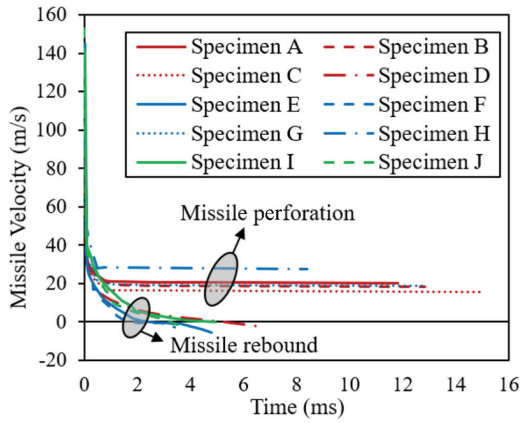

Fig. 8—Analytical missile velocity-time responses.

reinforcement. Specimens B, C, E, F, I, and J had 26.5 mm (1.04 in.) diameter prestressing bars spaced at 180 mm (7.09 in.), placed in plastic sleeves. Details of the specimens are summarized in Table 1.

The modeling approach was the same as that used for the VTT-P1 specimen. The prestressing reinforcement was modeled with 250 discrete truss elements connected to the nodes with linkage elements. Therefore, the prestressing reinforcement was modeled as unbonded by providing a low bond stress for the linkage elements. An updated damping matrix was used in the analyses, and the same erosion limit was used for both element erosion criteria. The average of initial damping ratios for the first and second modes were 3.1 and 10.5%, respectively. The element erosion limit obtained from the self-calibration procedure varied from 0.15 to 0.30 for the 10 specimens.

The computed missile velocity-time histories are shown in Fig. 8. The analyses were stopped at the time steps when either the front of the missile perforated through the back of the target or the missile velocity became negative, indicating a rebound of the missile. According to the analytical responses, the missile perforated through Specimens A, B, C, G, and H with residual velocities ranging from 15.8 to 27.5 m/s (51.8 to 90.2 ft/s). For Specimens A, B, and C, the missiles were stopped by the targets in the tests, leaving holes with depths of up to 130 mm (5.12 in.), indicating severe deformation due to punching behavior. For Specimens G and H, the missiles perforated with residual velocities of 21 and 30 m/s (68.9 and 98.4 ft/s), which were reasonably close to the values computed by the analyses.

Table 1—Summary of specimens tested by Orbovic et al.[23] and Orbovic and Blahoianu[24]

Specimen	Missile velocity, m/s	Concrete compressive strength, MPa	Reinforcement		Prestressing, MPa
			In-plane	Out-of-plane	
A	103	48.3	✓	x	x
B	102	52.1	✓	x	5
C	99	48.7	✓	x	10
D	100	45.0	✓	✓	x
E	98	45.8	✓	✓	5
F	98	45.0	✓	✓	10
G	110	50.3	✓	x	x
H	144	53.0	✓	✓	x
I	139	50.0	✓	✓	10
J	153	62.9	✓	✓	10

Note: 1 m/s = 3.281 ft/s; 1 MPa = 0.145 ksi.

For specimens D, E, F, I, and J, the velocities of the missiles computed by the analyses continuously decreased and became negative, indicating rebounding of the missile. For Specimen D, the impact depth calculated from the analysis was 33 mm (1.30 in.), closely matching the test observation of 38 mm (1.50 in.). For Specimens E and F, the experimentally observed impact depths were 47 and 75 mm (1.85 and 2.95 in.), respectively, which were larger than the results obtained from the analyses. However, the increase in the impact depths was not expected because Specimens E and F had additional prestressing reinforcement compared to Specimen D, and the initial missile velocities were slightly lower. Therefore, the impact depths in Specimens E and F were expected to be smaller than that in Specimen D, as observed in the analyses.

For Specimens I and J, the missile velocities computed by the analyses became negative, indicating rebounding as was observed in the experiments. Although the missiles rebounded, the specimens were severely damaged. For Specimen I, a small hole through the cross section of the slab was observed in the experiment. Similarly, most of the

elements along the cross section adjacent to the target area eroded in the analysis.

In both the analyses and the experiments, the level of damage to the slabs significantly decreases with the presence of transverse reinforcement and prestressing bars. The deformed geometries and damage surfaces obtained from the analyses and tests for Specimens B, D, and E, each having different reinforcement details, are compared in Fig. 9.

The damaged surfaces of Specimens G and H, in which the missiles perforated through the slabs, are also presented in Fig. 9. For both specimens, the damaged surfaces on the front faces obtained from the analyses were larger than those observed experimentally, as with the VTT-P1 specimen. The coarseness of the mesh size, which influences the size of the area depleted by element erosion, maybe the possible cause of this. At the back face of Specimen G, the damaged surface in the horizontal direction was significantly larger than that in the vertical direction. Orbovic et al.[23] attributed this to pullout of the reinforcement and to differences between the support conditions in the vertical and horizontal directions. In the analyses, because the reinforcing bars in both directions were modeled at the same level, and because the support conditions were the same for both directions, the damage surface was symmetric about both axes. For Specimen H, the experimentally observed damage levels in the horizontal and vertical directions at the back face were close to each other, and also consistent with the analysis results.

The analytical and experimental results of all specimens are summarized in Table 2. It can be seen that the analytical model was able to capture the extent and mode of damage of almost all specimens with reasonable accuracy. In particular, the residual velocity of perforated specimens subjected to hard missiles and the maximum displacement of the specimen under soft missile were predicted very well. For specimens with no out-of-plane reinforcement, however, the model had a tendency to overestimate the damage.

CONCLUSIONS

The aim of this study was to develop a macro-modeling method for the analysis of reinforced and prestressed concrete slabs subjected to soft or hard missile impacts. Based on a series of verification studies performed on 12 impact test specimens with a wide range of concrete compressive strength and reinforcement configurations and a series of parametric analytical studies, the following conclusions can be made:

1. The macro-modeling analysis method proposed, using a smeared rotating crack model for concrete and a total-load secant stiffness solution algorithm based on the Modified Compression Field Theory, is a viable alternative for modeling soft- and hard-missile on concrete slabs.

2. The analytical and experimental results were generally in good agreement in terms of the maximum displacement, residual velocity, impact depth, failure mode, and scabbing area. For the hard-missile impact tests, the analyses were able to capture the shear mechanisms, including the shear cone observed in the test specimens. The effects of prestressing and shear reinforcement on the structural response were also captured well. However, the level of damage for slab specimens with no out-of-plane reinforcement was overestimated. Also, the analyses resulted in

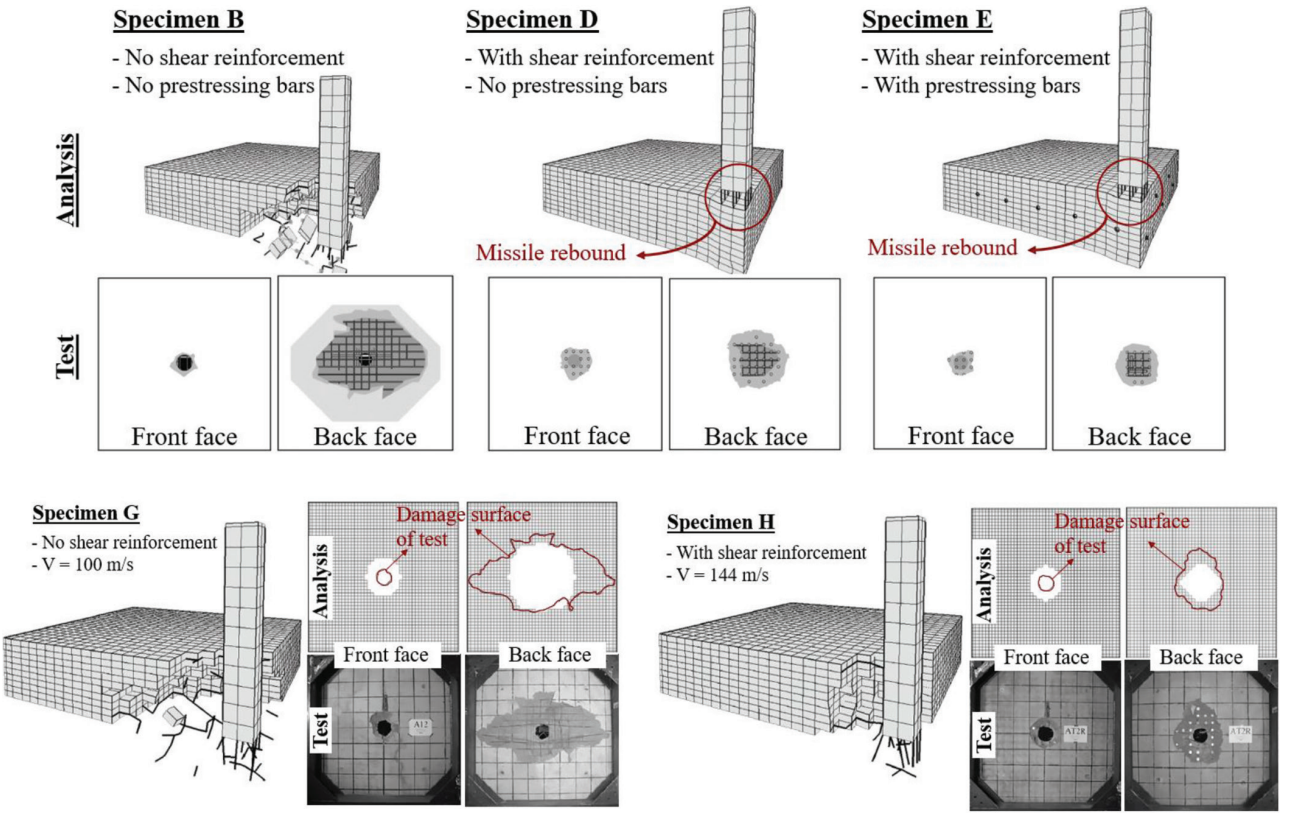

Fig. 9—Analytical and experimental damage surfaces for Specimens B, D, E, G, and H.

Table 2—Summary of analytical and experimental results

Specimen		Experimental damage mode		Analytical damage mode	
Reinforced concrete	VTT-B1	Flexural cracking	MD = 28.87 mm	Flexural cracking	MD = 29.03 mm
	VTT-P1	Perforation	RV = 33.8 m/s	Perforation	RV = 31.8 m/s
Prestressed concrete	A	Severe punching	ID = 120 mm	Perforation	RV = 20.1 m/s
	B	Severe punching	ID = 130 mm	Perforation	RV = 18.5 m/s
	C	Severe punching	ID = 110 mm	Perforation	RV = 15.8 m/s
	D	Spalling	ID = 38 mm	Spalling	ID = 33 mm
	E	Spalling	ID = 47 mm*	Spalling	ID = 21 mm
	F	Spalling	ID = 74 mm*	Spalling	ID = 13 mm
	G	Perforation	RV = 21 m/s	Perforation	RV = 18.4 m/s
	H	Perforation	RV = 30 m/s	Perforation	RV = 27.5 m/s
	I	Severe punching	ID = N/A	Severe punching	ID = 51 mm
	J	Severe punching	ID = N/A	Severe punching	ID = 31 mm

*Seems to be too high. Refer to "Verification Studies" section for more information.

Note: MD is maximum displacement (mm); RV is residual velocity (m/s); ID is impact depth (mm); 1 mm = 0.0394 in.; 1 m/s = 3.281 ft/s.

slightly larger spalling areas with lower impact depths than those experimentally observed.

3. To accurately capture local damage in hard missile impact tests, the in-plane reinforcement should be modeled with discrete truss elements; otherwise, element erosion may cause excessive loss of reinforcing steel. Additionally, modeling the in-plane reinforcement with discrete truss bar elements allows the monitoring of the damage condition of each reinforcing bar.

4. Considering strain rate effects for both the concrete and reinforcing steel produced unconservative results. The inertial effects and triaxial confinement stress conditions of concrete that are typically induced under dynamic loads will naturally result in elevated strengths. Therefore, considering strain rate effects for only the reinforcing steel is recommended when using the proposed analysis procedure or other similar finite element (FE) analysis methods.

5. The iterative self-calibrating procedure is a reliable approach to systematically determine proper damping ratios and element erosion limits for the analysis of concrete slabs under impact loading. Erosion limits within the range of 0.15 to 0.30 for the shear strain and principal tensile strain are suitable for modeling hard missile impact tests.

6. Compared to the constant damping method, the updating damping method found to be a more effective approach to satisfy numerical stability without causing excessive damping in the system. By updating the damping matrix in every load step, the damping effects diminish quickly, allowing the use of higher initial damping ratios. In hard missile impact analyses, using a constant damping matrix, even with small damping coefficients, causes the inclusion of excessive energy dissipating mechanisms.

7. The proposed FE analysis method provides the same level of accuracy as the hydrocode approaches, but with much less computational and modeling efforts without requiring extensive characterization of material properties or calibration of analysis parameters.

AUTHOR BIOS

Andac Lulec *is an Engineer in Training at BBA Inc., Toronto, ON, Canada. He received his PhD from the University of Toronto, Toronto, ON, Canada, in 2017. His research interests include analysis of reinforced concrete structures under impact and blast loads.*

Vahid Sadeghian *is an Assistant Professor at the Department of Civil and Environmental Engineering at Carleton University, Ottawa, ON, Canada. His research interests include design and performance assessment of concrete structures, modeling of concrete structures under extreme loading, and hybrid (experimental-numerical) simulation.*

Frank J. Vecchio*, FACI, is a Professor in the Department of Civil Engineering at the University of Toronto. He is a member of Joint ACI-ASCE Committees 441, Reinforced Concrete Columns, and 447, Finite Element Analysis of Reinforced Concrete Structures. His research interests include nonlinear analysis and design of reinforced concrete structures, constitutive modeling, performance assessment and forensic investigation, and repair and rehabilitation of structures.*

REFERENCES

1. Lulec, A.; Sadeghian, V.; and Vecchio, F. J., "Prediction of Perforation Velocity of Hard Missile Impacts on Reinforced Concrete Wall Panels," *Canadian Journal of Civil Engineering*, V. 48, No. 1, 2021, pp. 26-38. doi: 10.1139/cjce-2019-0548

2. Teng, T. L.; Chu, Y. A.; Chang, F. A.; and Chin, H. S., "Simulation Model of Impact on Reinforced Concrete," *Cement and Concrete Research*, V. 34, No. 11, 2004, pp. 2067-2077. doi: 10.1016/j.cemconres.2004.03.019

3. Chung, C.; Lee, J.; and Jung, R., "Numerical Simulations of Missile Impacts on Reinforced Concrete Plates: IRIS-2010/2012 Benchmark Project," *Nuclear Engineering and Design*, V. 295, 2015, pp. 747-758. doi: 10.1016/j.nucengdes.2015.04.031

4. Vepsä, A., "Experimental Tests for Bending and Punching Behavior of Reinforced Concrete Walls under Impact Loading," Research *Report* VTT-R-05587-10, 2010, 172 pp.

5. Vepsä, A., "Punching Behavior of One 250 mm Thick Reinforced Concrete Wall under Hard Impact Loading: Revision A," Research *Report* VTT-05588-10, 2010, 71 pp.

6. Saatci, S., and Vecchio, F. J., "Nonlinear Finite Element Modeling of Reinforced Concrete Structures under Impact Loads," *ACI Structural Journal*, V. 106, No. 5, Sept.-Oct. 2009, pp. 717-725.

7. ElMohandes, F., and Vecchio, F. J., "User's Manual of VecTor3," University of Toronto, Toronto, ON, Canada, 2014, 153 pp.

8. Rayleigh, L., *The Theory of Sound*, Macmillan, London, UK, 1877.

9. Vecchio, F. J., "Disturbed Stress Field Model for Reinforced Concrete: Formulation," *Journal of Structural Engineering*, ASCE, V. 126, No. 9, 2000, pp. 1070-1077. doi: 10.1061/(ASCE)0733-9445(2000)126:9(1070)

10. Vecchio, F. J., and Collins, M. P., "The Modified Compression-Field Theory for Reinforced Concrete Elements Subjected to Shear," *ACI Journal Proceedings*, V. 83, No. 2, Mar.-Apr. 1986, pp. 219-231.

11. Lulec, A., "Simplified Analytical Tools for Impact and Impulsive Loading Analysis of Reinforced Concrete Structures," PhD thesis, University of Toronto, Toronto, ON, Canada, 219 pp.

12. Hoshikuma, J.; Kawashima, K.; Nagaya, K.; and Taylor, A. W., "Stress-Strain Model for Confined Reinforced Concrete in Bridge Piers," *Journal of Structural Engineering*, ASCE, V. 123, No. 5, 1997, pp. 624-633. doi: 10.1061/(ASCE)0733-9445(1997)123:5(624)

13. Vecchio, F. J., and Collins, M. P., "Compression Response of Cracked Reinforced Concrete," *Journal of Structural Engineering*, ASCE, V. 119, No. 12, 1993, pp. 3590-3610. doi: 10.1061/(ASCE)0733-9445(1993)119:12(3590)

14. Bentz, E. C., "Explaining the Riddle of Tension Stiffening Models for Shear Panel Experiments," *Journal of Structural Engineering*, ASCE, V. 131, No. 9, 2005, pp. 1422-1425. doi: 10.1061/(ASCE)0733-9445(2005)131:9(1422)

15. Walraven, J. C., "Fundamental Analysis of Aggregate Interlock," *Journal of the Structural Division*, ASCE, V. 107, No. 11, 1981, pp. 2245-2270. doi: 10.1061/JSDEAG.0005820

16. Palermo, D., and Vecchio, F. J., "Compression Field Modelling of Reinforced Concrete Subjected to Reversed Loading: Formulation," *ACI Structural Journal*, V. 100, No. 5, Sept.-Oct. 2003, pp. 616-625.

17. Seckin, M., "Hysteretic Behaviour of Cast-in-Place Exterior Beam-Column-Slab Subassemblies," PhD thesis, University of Toronto, Toronto, ON, Canada, 1981, 266 pp.

18. Akkaya, Y.; Guner, S.; and Vecchio, F. J., "Constitutive Model for Inelastic Buckling Behavior of Reinforcing Bars," *ACI Structural Journal*, V. 116, No. 2, Mar. 2019, pp. 195-204. doi: 10.14359/51711143

19. Comité Euro-International du Béton (CEB) and Fédération Internationale de la Précontrainte, (FIP), "Model Code 2010," *fib* Bulletin No. 65, Lausanne, Switzerland, 2012, 350 pp.

20. Malvar, L. J., and Crawford, J. E., "Dynamic Increase Factor for Steel Reinforcing Bars," *28th DDESB Seminar*, Orlando, FL, 1998.

21. Luccioni, B., and Aráoz, G., "Erosion Criteria for Frictional Materials under Blast Load," *Mecánica Computacional*, V. 30, 2011, pp. 1809-1831.

22. Riera, J. D., "On the Stress Analysis of Structures Subjected to Aircraft Impact Forces," *Nuclear Engineering and Design*, V. 8, No. 4, 1968, pp. 415-426. doi: 10.1016/0029-5493(68)90039-3

23. Orbovic, N.; Elgohary, M.; Lee, N.; and Blahoianu, A., "Tests on Reinforced Concrete Slabs with Pre-stressing and with Transverse Reinforcement under Impact Loading," *20th International Conference on Structural Mechanics in Reactor Technology (SMIRT20)*, Espoo, Finland, 2009.

24. Orbovic, N., and Blahoianu, A., "Tests on Concrete Slabs under Hard Missile Impact to Evaluate the Influence of Transverse Reinforcement and Pre-Stressing on Perforation Velocity," *21st International Conference on Structural Mechanic in Reactor Technology (SMIRT21)*, New Delhi, India, 2011.